X-ray Crystallographic and Biochemical Characterization of the Inhibitory Action of an Imidazole−Dioxolane Compound on Heme Oxygenase[†,‡]

Masakazu Sugishima,[§] Yuichiro Higashimoto,[§] Tohru Oishi,[||] Hidenori Takahashi,[⊥] Hiroshi Sakamoto,[@] Masato Noguchi,[§] and Keiichi Fukuyama*[,⊥]

Department of Medical Biochemistry, Kurume University School of Medicine, Kurume, Fukuoka 830-0011, Japan, Department of Chemistry and Department of Biological Sciences, Graduate School of Science, Osaka University, Toyonaka, Osaka 560-0043, Japan, and Department of Bioscience and Bioinformatics, Faculty of Computer Science and Systems Engineering, Kyushu Institute of Technology, Iizuka, Fukuoka 820-8502, Japan

Received November 2, 2006; Revised Manuscript Received December 7, 2006

ABSTRACT: Heme oxygenase (HO) catalyzes the regiospecific cleavage of the porphyrin ring of heme using reducing equivalents and O_2 to produce biliverdin, iron, and CO. Because CO has a cytoprotective effect through the p38-MAPK pathway, HO is a potential therapeutic target in cancer. In fact, inhibition of the HO isoform HO-1 reduces Kaposi sarcoma tumor growth. Imidazole−dioxolane compounds have recently attracted attention because they have been reported to specifically inhibit HO-1, but not HO-2, unlike Cr-containing protoporphyrin IX, a classical inhibitor of HO, that inhibits not only both HO isoforms but also other hemoproteins. The inhibitory mechanism of imidazole−dioxolane compounds, however, has not yet been characterized. Here, we determine the crystal structure of the ternary complex of rat HO-1, heme, and an imidazole−dioxolane compound, 2-[2-(4-chlorophenyl)ethyl]-2-[(1*H*-imidazol-1-yl)methyl]-1,3-dioxolane. This compound bound on the distal side of the heme iron, where the imidazole and 4-chlorophenyl groups were bound to the heme iron and the hydrophobic cavity in HO, respectively. Binding of the bulky inhibitor in the narrow distal pocket shifted the distal helix to open the distal site and moved both the heme and the proximal helix. Furthermore, the biochemical characterization revealed that the catalytic reactions of both HO-1 and HO-2 were completely stopped after the formation of verdoheme in the presence of the imidazole−dioxolane compound. This result should be mainly due to the lower reactivity of the inhibitor-bound verdoheme with O_2 compared to the reactivity of the inhibitor-bound heme with O_2.

Heme oxygenase (HO,[1] EC 1.14.99.3) catalyzes the O_2-dependent cleavage of the porphyrin ring of heme using reducing equivalents to produce biliverdin, iron, and CO (*1*). This reaction (Scheme 1) consists of three sequential oxidation steps (*2*−*4*). In the first step, O_2 bound to the heme iron is activated to become hydroperoxide, and electrophilic addition of its terminal oxygen to the α-*meso* carbon produces α-hydroxyheme. In the second step, α-hydroxyheme is converted to verdoheme with the concomitant release of the α-*meso* carbon as CO. Approximately 85% of CO produced under normal physiological conditions is derived from this reaction (*5*). Last, the oxygen bridge of verdoheme is cleaved to produce biliverdin−iron chelate, and the iron is released prior to the dissociation of biliverdin. In the reaction catalyzed by HO, heme acts as both substrate and cofactor.

Two isoforms of HO, HO-1 and HO-2, are present in mammals. Although it was previously reported that a third isoform, HO-3, is present in rats, recent genetic analysis revealed that *ho*3 is a pseudogene (*6*). HO-1 (32 kDa) is strongly expressed in spleen and liver, and its expression is induced by various substances, including heme itself. HO-1 mainly functions to maintain iron homeostasis and is involved in defending the body against oxidative stress by removing prooxidant, free heme, and by producing the antioxidants, biliverdin and bilirubin (*7*, *8*). In contrast, HO-2 (36 kDa) is expressed constitutively in brain, testis, and

[†] This work was supported in part by Grant-in-Aid for Young Scientists 18770121 (to Y.H.) and a grant of the National Project on Protein Structural and Functional Analyses from the Ministry of Education, Culture, Sports, Science, and Technology of Japan, by Grants-in-Aid for Scientific Research 18590278 (to M.N.), 18550153 (to H.S.), 18054016 (to K.F.), and 18570105 (to K.F.) and for Research Fellows 17-5063 (to M.S.) from the Japan Society for the Promotion of Science, by a grant from the Samurou Kakiuchi Foundation for the Promotion of Science (to H.S.), and by a grant from the Morikazu Kaibara Medical Science Promotion Foundation (to Y.H.).

[‡] Coordinates and structure factors of the ternary complex of rat HO-1, heme, and 2-[2-(4-chlorophenyl)ethyl]-2-[(1*H*-imidazol-1-yl)methyl]-1,3-dioxolane have been deposited in the Protein Data Bank as entry 2DY5.

* To whom correspondence should be addressed: Department of Biological Sciences, Graduate School of Science, Osaka University, 1-1 Machikaneyama, Toyonaka, Osaka 560-0043, Japan. Telephone: +81-6-6850-5422. Fax: +81-6-6850-5425. E-mail: fukuyama@bio.sci.osaka-u.ac.jp.

[§] Kurume University School of Medicine.

[||] Department of Chemistry, Graduate School of Science, Osaka University.

[⊥] Department of Biological Sciences, Graduate School of Science, Osaka University.

[@] Kyushu Institute of Technology.

[1] Abbreviations: CPR, NADPH-cytochrome P450 reductase; HO, heme oxygenase; heme−HO, HO in complex with heme; DIOCPI, 2-[2-(4-chlorophenyl)ethyl]-2-[(1*H*-imidazol-1-yl)methyl]-1,3-dioxolane.

10.1021/bi062264p CCC: $37.00
Published on Web 01/25/2007

Scheme 1: Reaction Scheme of HO

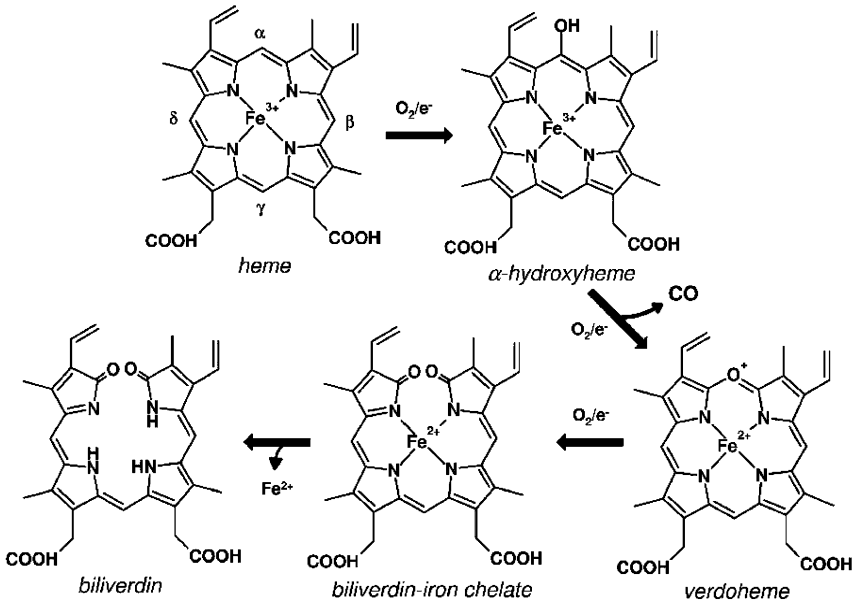

vascular systems. The principal role of HO-2 is supposed to be production of CO as a neurotransmitter (*9*, *10*).

A recent study suggested that CO produced by HO-1 has antiinflammatory, antiproliferative, and antiapoptotic effects (*11*), though the direct molecular targets of CO were not identified. Furthermore, it has been shown that the growth of most tumors depends on HO-1 (*12*) and that the tumor growth induced by the viral G protein-coupled receptor, which is expressed in AIDS-Kaposi sarcoma lesions, is suppressed by the inhibition of HO-1 and enhanced by the induction of HO-1 expression (*13*). Thus, HO-1 is a potential therapeutic target in cancer.

Imidazole−dioxolane compounds have recently attracted a great deal of attention because they exhibited high selectivity for the inhibition of HO activity in rat spleen microsomes compared to that in rat brain microsomes, suggesting that the inhibitors selectively inhibit HO-1 over HO-2 (*14*). Furthermore, imidazole−dioxolane compounds did not effectively inhibit the activities of nitric oxide synthase and soluble guanylyl cyclase though Cr-containing protoporphyrin IX, a classical inhibitor of HO, inhibits not only the HO isoforms but also these hemoproteins (*15*). The mechanism employed by the imidazole−dioxolane compounds to inhibit the activity of HO, however, has not yet been characterized.

Here, we determine the crystal structure of the ternary complex of rat HO-1, heme, and the imidazole−dioxolane compound, 2-[2-(4-chlorophenyl)ethyl]-2-[(1*H*-imidazol-1-yl)methyl]-1,3-dioxolane (DIOCPI). Additionally, we biochemically characterized the mechanism by which this compound inhibits the HO reaction. Our results revealed that the imidazole−dioxolane compound bound to the distal side of the heme iron in HO and completely inhibited both HO isoforms from converting verdoheme to biliverdin and provide the structural basis for the design of HO-specific inhibitors.

MATERIALS AND METHODS

Chemical Synthesis of DIOCPI. DIOCPI (*16*) was prepared from 4-(4-chlorophenyl)-1-(1*H*-imidazol-1-yl)-2-butanone

Scheme 2 [a]

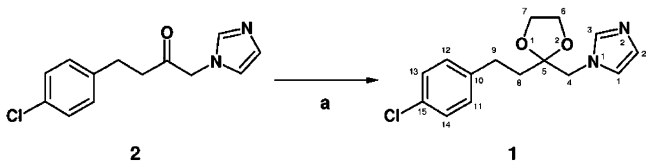

[a] Reagents and conditions: (a) ethylene glycol, *p*-toluenesulfonic acid monohydrate, toluene, reflux, 4 h.

(*14*, *17*) by forming a ketal with ethylene glycol using *p*-toluenesulfonic acid (Scheme 2) (*18*). A 0.40 mmol solution of 4-(4-chlorophenyl)-1-(1*H*-imidazol-1-yl)-2-butanone (100 mg) in toluene (5 mL) was mixed with 4.0 mmol of ethylene glycol (223 μL) and 0.80 mmol of *p*-toluenesulfonic acid monohydrate (76 mg), and the mixture was heated at reflux for 4 h. After cooling to room temperature, the reaction mixture was poured into saturated aqueous $NaHCO_3$ in ethyl acetate while being stirred at 0 °C and extracted with ethyl acetate. The combined organic layers were washed with saturated aqueous NaCl and dried over anhydrous $MgSO_4$. Concentration was followed by silica gel column chromatography (chloroform/methanol) to give DIOCPI (72.5 mg, 0.25 mmol, 63%) as a colorless solid: ^{1}H NMR (500 MHz, $CDCl_3$) δ 7.47 (1H, s), 7.22 (2H, d, J = 8.5 Hz), 7.08 (2H, d, J = 8.5 Hz), 3.98 (2H, s), 3.85 (2H, m), 3.46 (2H, m), 2.67 (2H, m), 1.89 (2H, m); ESI-MS *m*/*z* 293 ($M + H^+$).

Enzymes. Truncated rat HO-1 (Met 1−Pro 267) was prepared as described previously (*19*). The cDNA for a soluble form of rat HO-2 (Met 1−Ala 288) was amplified with a sense primer (5′-AACTCAGCACATATGTCTTCAGAGGTGGA-3′) and an antisense primer (5′-GCTAGGCTTGGATCCTTAAGCCATG-3′) using a rat liver cDNA library (Invitrogen, Carlsbad, CA). The PCR-amplified fragments were cloned into the *Nde*I−*Bam*HI sites of the pET-11a expression vector. The resulting plasmid was transformed into *Escherichia coli* BLR(DE3) cells, and the cells were grown in LB medium with 50 μg/mL ampicillin at 37 °C. When the OD_{600} of the culture reached 0.5−0.6, IPTG was added to a final concentration of 1 mM and the

culture was further incubated at 37 °C for 3 h with shaking. The harvested cells were sonicated, and the membrane fraction was removed by centrifugation. The cell lysate was purified by two-step column chromatography on hydroxylapatite and POROS-HQ columns, according to the procedures used to prepare truncated rat HO-1 (*19*), except that all buffers contained 0.4 mM DTT. The purified enzyme resulted in a single protein band of 33 kDa following SDS−PAGE. The final preparations of rat HO-1 and rat HO-2 had specific activities of 8413 ± 283 and 4712 ± 459 units/mg of protein, respectively; 1 unit represents the amount of enzyme that catalyzes the formation of 1 nmol of bilirubin/h under the usual assay conditions (*20*). The enzyme activities of recombinant rat HO-1 and HO-2 were comparable to those reported in previous studies (*19*, *21*). Recombinant rat liver NADPH-cytochrome P450 reductase (CPR) that lacked the 57 N-terminal hydrophobic amino acids was expressed and purified as previously described (*22*).

The ferric heme complexes of rat HO-1 and rat HO-2 were purified by hydroxylapatite column chromatography after mixing 1.2 equiv of heme with the enzyme (*20*). The ferrous heme complexes were prepared by reducing the ferric form of the complexes with a stoichiometric amount of sodium dithionite under anaerobic conditions.

The reconstitution and purification of the complexes of verdoheme with rat HO-1 and HO-2 were performed as reported previously (*23*).

Inhibitor Binding Study. Inhibitor binding studies were performed in an anaerobic glovebox at room temperature (25 °C). Aliquots of DIOCPI dissolved in 1 mM DMSO were added to 5 μM ferric or ferrous heme−HO complexes. Spectra were recorded after each addition of DIOCPI. Titration curves were constructed by plotting the absorbance at 414 nm (for a ferric heme−HO complex) or 423 nm (for a ferrous heme−HO complex) against the amount of DIOCPI added (0.2−10 μM) and analyzed using Deltagraph (DeltaPoint, Monterey, CA).

Preparation of Crystals of the Ternary Complex of Rat HO-1, Heme, and DIOCPI. The ferric heme−HO-1 complex was crystallized under aerobic conditions similar to those used for the azide-bound heme−HO-1 complex (*24*). The microseeding technique was used to improve the diffraction quality of the crystals. DIOCPI-bound crystals were prepared by soaking crystals in a crystallization solution containing 1 mM DIOCPI and 5% (v/v) DMSO. After being soaked for 1 min, a DIOCPI-bound crystal mounted on a cryoloop was immediately cooled with liquid nitrogen. Crystals were broken when soaked over a few minutes or in the DIOCPI solution at a higher concentration.

Determination of the Structure of the Ternary Complex. Diffraction data were collected at 100 K using the synchrotron radiation (λ = 1.0000 Å) at the BL41XU beamline of SPring-8 and the ADSC Quantum315 detector. Diffraction data were processed and scaled with HKL2000 (*25*). The crystal belonged to space group $P3_221$ with the following unit cell dimensions: $a = b = 66.2$ Å and $c = 121.0$ Å. The structure of the DIOCPI-bound form of the complex was determined using the molecular replacement method with MolRep (*26*) and the protein moiety of the azide-bound heme−HO-1 structure (PDB entry 1IVJ) (*24*) as a search model. Rotational and translational searches using the diffraction data (15−4.0 Å) identified one molecule in an asymmetric unit. The respective correlation coefficient and *R*-factor for the correct solution were 0.684 and 0.411, respectively, whereas those for the second unrelated peak were 0.318 and 0.594, respectively. The structure of the protein moiety was refined with CNS (*27*). The resultant $F_o - F_c$ electron density map showed significant electron density for the heme and DIOCPI. Then, heme and DIOCPI were added to the model and refined. The structure of the tetrapyrrole moiety of heme was restrained in a planar conformation, and the distances between the heme iron and the nitrogen atoms of the imidazole rings of His 25 and DIOCPI were weakly restrained to 2.0 Å in the refinements (10 kcal/mol). Finally, several water molecules and a chloride ion were added to the model and refined. Diffraction and refinement statistics are summarized in Table 1.

Table 1: Diffraction and Refinement Statistics

diffraction statistics[a]	
resolution (Å)	50−2.70
no. of observations	66326
no. of unique reflections	8774
completeness (%)	97.4 (93.1)
mean $I_o/\sigma(I)$	10.6
R_{sym}[b] (%)	9.1 (31.9)
refinement statistics	
R^c/R_{free}[d] (%)	19.4/24.6
no. of protein atoms	1742
no. of ligand atoms (heme and DIOCPI)	43/20
no. of solvent molecules (Cl^- and H_2O)	1/10
average atomic *B*-factor (Å^2) (protein/ligands/solvent molecules)	48.9/53.1/47.9
rms deviations from ideal values	
bond lengths (Å)	0.01
bond angles (deg)	1.22
Ramachandran plot	
most favored (%)	91.6
additionally allowed (%)	8.4

[a] Values in parentheses correspond to the highest-resolution shell (2.80−2.70 Å). [b] $R_{sym} = \sum_{hkl}\sum_i|I_i(hkl) - \langle I(hkl)\rangle|/\sum_{hkl}\sum_i I_i(hkl)$. [c] $R = \sum_{hkl}||F_o(hkl)| - |F_c(hkl)||/\sum_{hkl}|F_o(hkl)|$. [d] R_{free} value calculated for 5% of the data set not included in the refinement.

Single-Turnover HO Reaction with Rat Heme−HO Complexes. All single-turnover reactions were monitored by optical absorption changes at 25 °C using a Varian Cary 50 Bio UV−visible spectrophotometer. Briefly, the reaction mixtures (0.1 mL) contained 5 μM heme−rat HO-1 or heme−rat HO-2 complexes, 0.04 μM CPR, and 25 μM NADPH in 0.1 M potassium phosphate buffer (pH 7.4) in the presence or absence of 25 μM DIOCPI. Spectra were recorded in the range of 300−900 nm.

RESULTS

Binding of Inhibitor to the Ferric and Ferrous Heme−HO Complexes. First, we examined the binding of DIOCPI to the complexes of heme and recombinant rat HO-1 or HO-2 proteins. Under anaerobic conditions, the addition of an excess amount of DIOCPI to the ferric heme−rat HO-1 complex at pH 7.4 caused a Soret shift from 405 to 414 nm, indicating that DIOCPI directly interacted with the ferric heme iron. Titration studies revealed DIOCPI bound tightly to the ferric heme−rat HO-1 complex with a dissociation

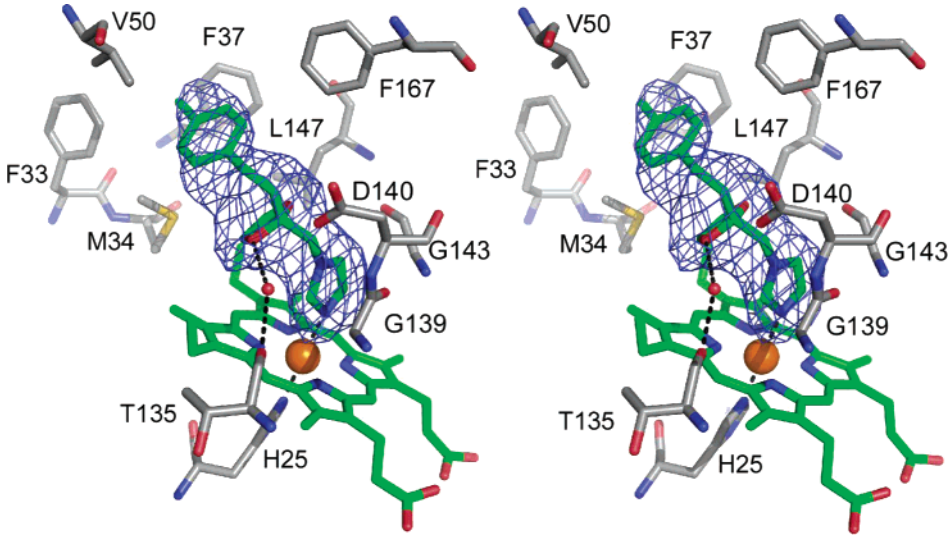

FIGURE 1: Stereodiagrams of the mode of binding of DIOCPI to rat heme-HO-1. A simulated annealing omit map of DIOCPI contoured at 4.0σ is superimposed on the model. Heme, His 25, and the residues involved in the binding of DIOCPI are shown as stick models. The coordination bonds of the heme iron and the hydrogen bond to DIOCPI are shown as dashed lines.

constant of 0.2 μM. The anaerobic addition of an excess amount of DIOCPI to the ferric heme−rat HO-2 complex produced an absorption spectral change similar to that observed for the ferric heme−rat HO-1 complex. DIOCPI, however, had a 5-fold lower binding affinity for the ferric heme−rat HO-2 complex; the dissociation constant was 0.9 μM.

Interestingly, DIOCPI also bound stoichiometrically to the ferrous forms of the heme−rat HO-1 and heme−rat HO-2 complexes under anaerobic conditions. The addition of an excess amount of DIOCPI to the complexes of ferrous heme and rat HO-1 or HO-2 at pH 7.4 caused a Soret shift from 430 to 423 nm. The dissociation constants of DIOCPI were 0.5 and 1.0 μM for the ferrous forms of the heme−rat HO-1 and heme−rat HO-2 complexes, respectively. These results indicate that DIOCPI has similar affinities to those of O_2 or CO for the ferric and ferrous forms of the heme−rat HO-1 and heme−rat HO-2 complexes (*28*).

Structure of the Ternary Complex of Rat HO-1, Heme, and DIOCPI. To investigate the detailed mode of binding of the imidazole−dioxolane compound to the heme−HO complex, we determined the crystal structure of the ternary complex of rat HO-1, heme, and DIOCPI at a resolution of 2.7 Å. The structure has a number of α-helices and is similar to the previously reported structure of rat HO-1 in complex with heme (*29*). The electron density map clearly shows that DIOCPI is bound on the distal side of the heme (Figure 1 and Figure S1 of the Supporting Information). The contacts between the heme−HO-1 complex and DIOCPI are listed in Table 2. The imidazole ring of DIOCPI is coordinated to the heme as was indicated by the optical spectrum of the heme−HO-1 complex in the presence of DIOCPI. The mode of binding of the imidazole ring to the heme iron in the complex presented here is similar to that in the ketoconazole−cytochrome P450 complex (*30*, *31*). The 4-chlorophenyl group of DIOCPI is bound to the hydrophobic cavity in the distal heme pocket, wherein the CO released from the CO-bound heme−HO-1 complex following photolysis was trapped and xenon was bound under a high-pressure xenon atmosphere (*32*). The water molecule that is hydrogen bonded to the carbonyl group of Thr 135 is weakly hydrogen bonded to the oxygen atom of the dioxolane group of DIOCPI. In addition, the dioxolane group interacts hydrophobically with Leu 147 and the heme. Thus, hydrophobic interactions and coordination bonding are responsible for the binding of DIOCPI to the heme−HO-1 complex.

Table 2: Contacts between the Heme−HO-1 Complex and DIOCPI[a]

atom of heme−HO-1/atom of DIOCPI	distance (Å)
Phe 33 Cϵ/Cl	3.7
Met 34 Cϵ/C14	3.6
Phe 37 Cδ/Cl	3.5
Val 50 Cγ/C14	3.6
Gly 139 O/N1	3.2
Asp 140 Oδ/C4	3.3
Gly 143 C/C1	3.4
Leu 147 Cδ/C7	3.3
Phe 167 Cζ/C12	3.5
heme Fe/N2	2.2

[a] Residues less than 3.8 Å from DIOCPI are listed. Atom names of DIOCPI refer to Scheme 2.

A structural comparison of the rat ferric heme−HO-1 complex and its DIOCPI-bound form is shown in Figure 2. In the rat ferric heme−HO-1 complex, a water/hydroxide ion is coordinated to the distal side of the heme iron, and the carbonyl group of Gly 139 and the amide group of Gly 143 are hydrogen bonded to this water/hydroxide ion (*24*, *29*). Once DIOCPI had bound, the conformation of the main chain of Ser 142 and Gly 143 changed and the bending angle of the distal helix changed to open the distal heme pocket. Although a similar structural change of the distal helix is observed in the biliverdin−iron chelate-bound form of rat HO-1 (*33*), the helical structure of the bending point of the distal helix (Gly 143−Gln 145) is disrupted in the DIOCPI-bound form. In addition to the change in the distal helix, the heme and the proximal helix were shifted approximately 0.8 Å toward the α-*meso* carbon along the α−γ axis of the heme. Similar structural changes of the heme and the proximal helix are observed in the CO- and CN^--bound forms of the rat heme−HO-1 complex (*34*). These structural changes in the heme pocket allow the structure to accommodate the bulky inhibitor in the narrow distal pocket.

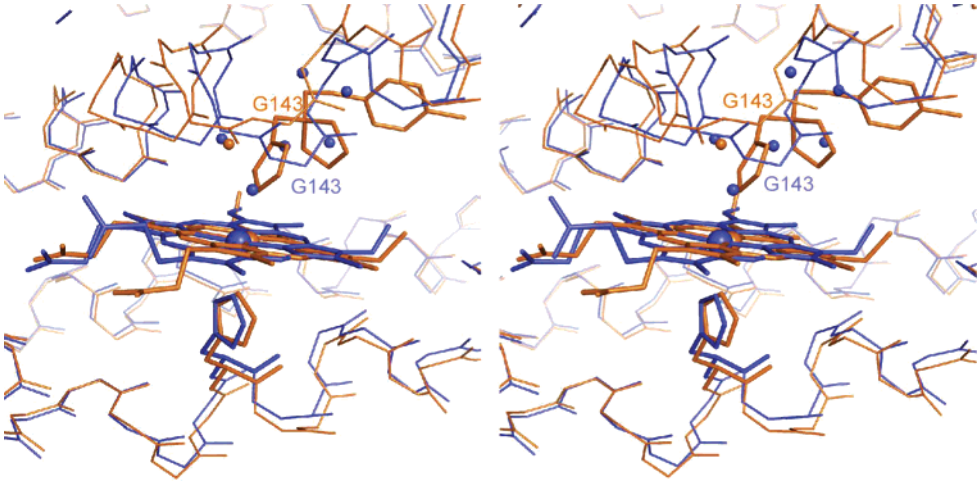

FIGURE 2: Stereodiagrams of the rat heme−HO-1 complex and rat heme−HO-1 complex bound to DIOCPI. The structure of the DIOCPI-bound form of the rat heme−HO-1 complex (orange) is superimposed on the structure of the rat heme−HO-1 complex (blue, PDB entry 1DVE) to minimize the rms differences of the positions of the Cα atoms (rms difference = 0.83 Å for 214 residues). Heme, DIOCPI, and His 25 are shown as stick models. Only the main chain is shown for the other residues. Water molecules that are involved in the hydrogen bond network in the distal heme pocket of the rat heme−HO-1 complex and the water molecule hydrogen bonded to DIOCPI in DIOCPI-bound forms are also shown.

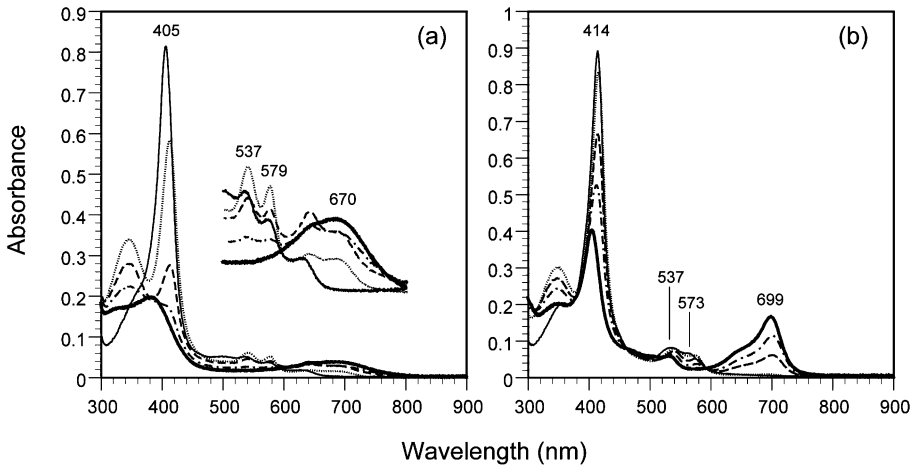

FIGURE 3: Absorption spectral changes of the heme−rat HO-1 complex during the NADPH/CPR-supported single-turnover reaction. The spectra were recorded before (—) and after the addition of NADPH [1 (•••), 5 (- - -), 10 (-•-), and 30 min (thick line)]: (a) without DIOCPI and (b) in the presence of 25 μM DIOCPI.

Single-Turnover Reactions of the Complexes of Heme and Rat HO-1 or HO-2. To further investigate the effect of DIOCPI on heme degradation, we measured absorption spectral changes during the HO reaction in air. The single-turnover NADPH/CPR-supported reaction of the heme−rat HO-1 complex is shown in Figure 3a. The heme complexed with rat HO-1 immediately changed to the ferrous oxy form upon addition of NADPH and CPR, which was indicated by the appearance of the 537 and 579 nm peaks. The ferrous oxy form was then transformed to biliverdin as indicated by the decrease in the Soret band and the increase in the absorption at approximately 670 nm. The heme bound to rat HO-1 was completely degraded to biliverdin within 30 min under these conditions.

Figure 3b shows the single-turnover NADPH/CPR-supported reaction of the heme−rat HO-1 complex in the presence of DIOCPI. Upon addition of NADPH and CPR, the intensity of the 414 nm Soret band slowly decreased and the band shifted to 405 nm. In the visible region, new absorption peaks at 537 and 573 nm, which corresponded to the oxy form of the heme−rat HO-1 complex, appeared within 5 min and then decreased in intensity along with the appearance of a new peak at 699 nm after 30 min. No additional spectral changes were observed after 60 min. The rate of conversion of heme to verdoheme was preliminarily estimated by the initial rate of the decrease of the magnitude of the Soret band (Figure S2). In the absence of DIOCPI, the conversion rate was 1.04 μM/min, whereas in the presence of DIOCPI, it was 0.33 μM/min. When CO gas was introduced into the 60 min reaction mixture, the magnitude of the 699 nm peak decreased and that of a clear peak at 643 nm increased. Thus, we concluded that the species that resulted in the 643 and 699 nm peaks were the CO ferrous and DIOCPI-bound ferrous forms of verdoheme, respectively (Figure S3).

To further confirm that the product formed in the single-turnover reaction with DIOCPI was the DIOCPI-bound verdoheme−HO-1 complex, we reconstructed the ferrous verdoheme−rat HO-1 complex. Under anaerobic conditions, the addition of an excess amount of DIOCPI to the ferrous verdoheme−rat HO-1 complex at pH 7.4 caused the peaks at 399 and 688 nm to shift to 405 and 699 nm, respectively

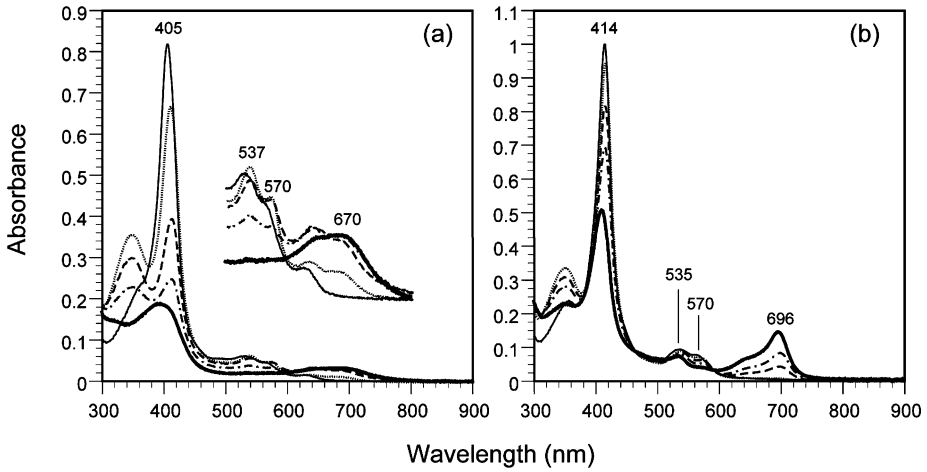

FIGURE 4: Absorption spectral changes of the heme−rat HO-2 complex during the NADPH/CPR-supported single-turnover reaction. The spectra were recorded before (—) and after the addition of NADPH [1 (•••), 5 (- - -), 10 (-•-), and 30 min (thick line)]: (a) without DIOCPI and (b) in the presence of 25 μM DIOCPI.

(Figure S4). The spectrum is identical to the final spectrum observed for the single-turnover reaction of the heme−rat HO-1 complex in the presence of DIOCPI. DIOCPI is bound to the ferrous verdoheme−rat HO-1 complex with a dissociation constant of 1.0 μM.

We next evaluated the inhibitory effect of DIOCPI for rat HO-2. Figure 4a shows the changes in the absorption spectrum during the NADPH/CPR-supported reaction of the heme−rat HO-2 complex in air. The spectrum of the heme−rat HO-2 complex following the addition of NADPH indicated that the heme was in the oxy form and then was transformed to biliverdin. The rate of degradation of the heme in rat HO-2 was somewhat slower than that of the heme in rat HO-1, which reflects the difference in the specific activities of rat HO-1 (8413 ± 283 units/mg of protein) and rat HO-2 (4712 ± 459 units/mg of protein). Figure 4b shows the changes in the absorption spectrum during the NADPH/CPR-supported reaction of the heme−rat HO-2 complex in the presence of DIOCPI. The spectral changes were almost identical to those observed for the heme−rat HO-1 complex in the presence of DIOCPI. Finally, ∼16.6% of heme in complex with rat HO-2 remained after the 60 min reaction. The product of the 60 min reaction was confirmed to be the DIOCPI-bound ferrous verdoheme−rat HO-2 complex (Figure S4). The dissociation constant of DIOCPI was 2.4 μM for the ferrous verdoheme−rat HO-2 complex.

These findings indicate that DIOCPI can bind to heme and verdoheme in complex with rat HO-1 and rat HO-2. Moreover, HO reactions in the presence of DIOCPI were completely terminated after the formation of verdoheme. This was likely due to the lower reactivity of DIOCPI-bound verdoheme with O_2 compared to the reactivity of DIOCPI-bound heme with O_2.

DISCUSSION

It has been reported that DIOCPI is a better inhibitor of HO activity in spleen microsomes compared to that in brain microsomes; the IC_{50} for spleen microsomes is 2.8 μM, whereas that for brain microsomes is >100 μM (*15*). These results suggest that DIOCPI selectively inhibits HO-1 over HO-2. Our study, however, clearly showed that DIOCPI is an equally effective inhibitor of HO-1 and HO-2. The structure of the ternary inhibitor complex of HO-1 supports our biochemical evidence. The structure of HO-2, which has not yet been determined, is likely to be similar to that of HO-1 because of the high degree of similarity in the amino acid sequences of these two isoforms. Although Met 34, Val 50, and Phe 167 in HO-1 are substituted in HO-2 with Val, Ala, and Tyr, respectively (Figure S5), the affinities of DIOCPI for HO-1 and HO-2 are expected to be similar. The IC_{50} reported in the previous study for the HO activity in spleen microsomes agreed with the affinity of DIOCPI for the ferrous heme−HO-1 complex, whereas the IC_{50} reported for the HO activity in brain microsomes did not concur with our result. Although the reason for this discrepancy is unclear at present, it might be related to the samples that were employed; purified recombinant proteins from rat were used in our assay, whereas tissue extracts from human were used in the previous study (*14*−*16*, *35*). In addition to the similarity of the structures of rat heme−HO-1 and human heme−HO-1 complexes (*29*, *36*), the residues involved in the binding of DIOCPI in rat HO-1 are completely conserved in human HO-1, and Met 34, Val 50, and Phe 167 in human HO-1 are substituted in human HO-2 in the same way that they are in rat HOs (Figure S5). Therefore, the use of either human HOs or rat HOs would bring about the same results and also would not give a clue about solving the discrepant results obtained with purified enzymes and microsomes.

We have shown the structural basis for the binding of imidazole−dioxolane compounds to HO. O_2 bound to the distal side of the heme becomes an active ferric hydrogen peroxide species, and then the α-*meso* carbon of heme is hydroxylated in the first step of the HO reaction. Asp 140 and the hydrogen bond network on the distal side of the heme are likely to have a prominent role in this reaction (*24*, *37*−*39*). The structure of the ternary complex demonstrated that the imidazole−dioxolane compound disrupts the hydrogen bond network and potentially competes with O_2 for binding to the ferrous heme iron (Figure 2). In fact, the rate of conversion of heme to verdoheme in HO-1 moderately decreased in the presence of DIOCPI (Figure S2).

Moreover, DIOCPI binds tightly to the ferrous verdoheme−HO complex as well as to the heme−HO complex. A recent study showed that the association rate constant for

binding of O_2 to the ferrous verdoheme−HO-1 complex (2.5×10^2 M^{-1} s^{-1}) was 4 orders of magnitude smaller than that for the heme−HO-1 complex (6.9×10^6 M^{-1} s^{-1}) (*28*, *40*). Together with these results, our findings indicate that complete inhibition of the HO reaction after the formation of verdoheme by DIOCPI is due to the low reactivity of the verdoheme−HO-1 complex with O_2.

The DIOCPI-bound structure determined in this study should be useful for the structure-based design of HO inhibitors. A previous study showed that (2*R*,4*R*)-2-[2-(4-chlorophenyl)ethyl]-2-[(1*H*-imidazol-1-yl)-methyl]-4-methyl-1,3-dioxolane, which has a methyl group added to the C4 position of the dioxolane group of DIOCPI, is more effective for the inhibition of HO activity in spleen microsomes (*15*). The structure presented here suggests that the addition of the methyl group to DIOCPI stabilizes the binding of the imidazole−dioxolane compound through hydrophobic interactions between the additional methyl group and heme, Met 34, and Leu 147. Electron density for DIOCPI showed that the imidazole and the dioxolane groups in HO-1 are ordered, whereas the chlorophenyl group is slightly disordered, although the chlorophenyl group appears to be involved in inhibitor binding through hydrophobic interactions. Drug design focused on the chlorophenyl moiety may produce a more effective and specific inhibitor of HO activity.

ACKNOWLEDGMENT

We thank Drs. Masahide Kawamoto and Nobutaka Shimizu of JASRI for their aid with data collection using the synchrotron radiation at SPring-8. We also thank Drs. Hiroyasu Yamaguchi, Hitoshi Yamamoto, and Michio Murata of Osaka University for advice about the preparation of DIOCPI.

SUPPORTING INFORMATION AVAILABLE

A $2F_o - F_c$ electron density map of the heme pocket of the ternary complex (Figure S1), absorption changes at the Soret band in the absence or presence of DIOCPI during the single-turnover reaction (Figure S2), absorption spectrum change of the reaction mixture in the presence of DIOCPI by the introduction of CO gas (Figure S3), spectra of the ferrous verdoheme−HO complex in the absence or presence of DIOCPI (Figure S4), and sequence alignment of HO-1 and HO-2 (Figure S5). This material is available free of charge via the Internet at http://pubs.acs.org.

REFERENCES

1. Tenhunen, R., Marver, H. S., and Schmid, R. (1968) The enzymatic conversion of heme to bilirubin by microsomal heme oxygenase, *Proc. Natl. Acad. Sci. U.S.A. 61*, 748−755.
2. Yoshida, T., and Migita, C. T. (2000) Mechanism of heme degradation by heme oxygenase, *J. Inorg. Biochem. 82*, 33−41.
3. Ortiz de Montellano, P. R. (2000) The mechanism of heme oxygenase, *Curr. Opin. Chem. Biol. 4*, 221−227.
4. Kikuchi, G., Yoshida, T., and Noguchi, M. (2005) Heme oxygenase and heme degradation, *Biochem. Biophys. Res. Commun. 338*, 558−567.
5. Rodgers, P. A., Vreman, H. J., Dennery, P. A., and Stevenson, D. K. (1994) Sources of carbon monoxide (CO) in biological systems and applications of CO detection technologies, *Semin. Perinatol. 18*, 2−10.
6. Hayashi, S., Omata, Y., Sakamoto, H., Higashimoto, Y., Hara, T., Sagara, Y., and Noguchi, M. (2004) Characterization of rat heme oxygenase-3 gene. Implication of processed pseudogenes derived from heme oxygenase-2 gene, *Gene 336*, 241−250.
7. Ryter, S. W., and Tyrrell, R. M. (2000) The heme synthesis and degradation pathways: Role in oxidant sensitivity. Heme oxygenase has both pro- and antioxidant properties, *Free Radical Biol. Med. 28*, 289−309.
8. Stocker, R., Yamamoto, Y., McDonagh, A. F., Glazer, A. N., and Ames, B. N. (1987) Bilirubin is an antioxidant of possible physiological importance, *Science 235*, 1043−1046.
9. Barañano, D. E., and Snyder, S. H. (2001) Neural roles for heme oxygenase: Contrasts to nitric oxide synthase, *Proc. Natl. Acad. Sci. U.S.A. 98*, 10996−11002.
10. Dioum, E. M., Rutter, J., Tuckerman, J. R., Gonzalez, G., Gilles-Gonzalez, M. A., and McKnight, S. L. (2002) NPAS2: A gas-responsive transcription factor, *Science 298*, 2385−2387.
11. Ryter, S. W., Alam, J., and Choi, A. M. (2006) Heme oxygenase-1/carbon monoxide: From basic science to therapeutic applications, *Physiol. Rev. 86*, 583−650.
12. Fang, J., Akaike, T., and Maeda, H. (2004) Antiapoptotic role of heme oxygenase (HO) and the potential of HO as a target in anticancer treatment, *Apoptosis 9*, 27−35.
13. Marinissen, M. J., Tanos, T., Bolos, M., de Sagarra, M. R., Coso, O. A., and Cuadrado, A. (2006) Inhibition of heme oxygenase-1 interferes with the transforming activity of the Kaposi sarcoma herpesvirus-encoded G protein-coupled receptor, *J. Biol. Chem. 281*, 11332−11346.
14. Vlahakis, J. Z., Kinobe, R. T., Bowers, R. J., Brien, J. F., Nakatsu, K., and Szarek, W. A. (2005) Synthesis and evaluation of azalanstat analogues as heme oxygenase inhibitors, *Bioorg. Med. Chem. Lett. 15*, 1457−1461.
15. Kinobe, R. T., Vlahakis, J. Z., Vreman, H. J., Stevenson, D. K., Brien, J. F., Szarek, W. A., and Nakatsu, K. (2006) Selectivity of imidazole-dioxolane compounds for in vitro inhibition of microsomal haem oxygenase isoforms, *Br. J. Pharmacol. 147*, 307−315.
16. Vlahakis, J. Z., Kinobe, R. T., Nakatsu, K., Szarek, W. A., and Crandall, I. E. (2006) Anti-*Plasmodium* activity of imidazole-dioxolane compounds, *Bioorg. Med. Chem. Lett. 16*, 2396−2406.
17. Walker, K. A., Kertesz, D. J., Rotstein, D. M., Swinney, D. C., Berry, P. W., So, O. Y., Webb, A. S., Watson, D. M., Mak, A. Y., Burton, P. M., et al. (1993) Selective inhibition of mammalian lanosterol 14α-demethylase: A possible strategy for cholesterol lowering, *J. Med. Chem. 36*, 2235−2237.
18. Walker, K. A. M. (1982) Derivatives of substituted N-alkylimidazoles, U.S. Patent 4321272.
19. Omata, Y., Asada, S., Sakamoto, H., Fukuyama, K., and Noguchi, M. (1998) Crystallization and preliminary X-ray diffraction studies on the water soluble form of rat heme oxygenase-1 in complex with heme, *Acta Crystallogr. D54*, 1017−1019.
20. Yoshida, T., and Kikuchi, G. (1979) Purification and properties of heme oxygenase from rat liver microsomes, *J. Biol. Chem. 254*, 4487−4491.
21. Trakshel, G. M., Kutty, R. K., and Maines, M. D. (1986) Purification and characterization of the major constitutive form of testicular heme oxygenase. The noninducible isoform, *J. Biol. Chem. 261*, 11131−11137.
22. Hayashi, S., Omata, Y., Sakamoto, H., Hara, T., and Noguchi, M. (2003) Purification and characterization of a soluble form of rat liver NADPH-cytochrome P-450 reductase highly expressed in *Escherichia coli*, *Protein Expression Purif. 29*, 1−7.
23. Sakamoto, H., Takahashi, K., Higashimoto, Y., Harada, S., Palmer, G., and Noguchi, M. (2005) A kinetic study of the mechanism of conversion of α-hydroxyheme to verdoheme while bound to heme oxygenase, *Biochem. Biophys. Res. Commun. 338*, 578−583.
24. Sugishima, M., Sakamoto, H., Higashimoto, Y., Omata, Y., Hayashi, S., Noguchi, M., and Fukuyama, K. (2002) Crystal structure of rat heme oxygenase-1 in complex with heme bound to azide: Implication for regiospecific hydroxylation of heme at the α-*meso* carbon, *J. Biol. Chem. 277*, 45086−45090.
25. Otwinowski, Z., and Minor, W. (1997) Processing of X-ray Diffraction Data Collected in Oscillation Mode, *Methods Enzymol. 276*, 307−326.
26. Vagin, A., and Teplyakov, A. (1997) MOLREP: An automated program for molecular replacement, *J. Appl. Crystallogr. 30*, 1022−1025.
27. Brünger, A. T., Adams, P. D., Clore, G. M., DeLano, W. L., Gros, P., Grosse-Kunstleve, R. W., Jiang, J. S., Kuszewski, J., Nilges, M., Pannu, N. S., Read, R. J., Rice, L. M., Simonson, T., and Warren, G. L. (1998) Crystallography & NMR system: A new

software suite for macromolecular structure determination, *Acta Crystallogr. D54*, 905−921.
28. Migita, C. T., Mansfield Matera, K., Ikeda-Saito, M., Olson, J. S., Fujii, H., Yoshimura, T., Zhou, H., and Yoshida, T. (1998) The oxygen and carbon monoxide reactions of heme oxygenase, *J. Biol. Chem. 273*, 945−949.
29. Sugishima, M., Omata, Y., Kakuta, Y., Sakamoto, H., Noguchi, M., and Fukuyama, K. (2000) Crystal structure of rat heme oxygenase-1 in complex with heme, *FEBS Lett. 471*, 61−66.
30. Cupp-Vickery, J. R., Garcia, C., Hofacre, A., and McGee-Estrada, K. (2001) Ketoconazole-induced conformational changes in the active site of cytochrome P450eryF, *J. Mol. Biol. 311*, 101−110.
31. Ekroos, M., and Sjogren, T. (2006) Structural basis for ligand promiscuity in cytochrome P450 3A4, *Proc. Natl. Acad. Sci. U.S.A. 103*, 13682−13687.
32. Sugishima, M., Sakamoto, H., Noguchi, M., and Fukuyama, K. (2004) CO-trapping site in heme oxygenase revealed by photolysis of its CO-bound heme complex: Mechanism of escaping from product inhibition, *J. Mol. Biol. 341*, 7−13.
33. Sugishima, M., Sakamoto, H., Higashimoto, Y., Noguchi, M., and Fukuyama, K. (2003) Crystal structure of rat heme oxygenase-1 in complex with biliverdin-iron chelate: Conformational change of the distal helix during the heme cleavage reaction, *J. Biol. Chem. 278*, 32352−32358.
34. Sugishima, M., Sakamoto, H., Noguchi, M., and Fukuyama, K. (2003) Crystal structures of ferrous and CO-, CN^--, and NO-bound forms of rat heme oxygenase-1 (HO-1) in complex with heme: structural implications for discrimination between CO and O_2 in HO-1, *Biochemistry 42*, 9898−9905.
35. Vlahakis, J. Z., Kinobe, R. T., Bowers, R. J., Brien, J. F., Nakatsu, K., and Szarek, W. A. (2006) Imidazole-dioxolane compounds as isozyme-selective heme oxygenase inhibitors, *J. Med. Chem. 49*, 4437−4441.
36. Schuller, D. J., Wilks, A., Ortiz de Montellano, P. R., and Poulos, T. L. (1999) Crystal structure of human heme oxygenase-1, *Nat. Struct. Biol. 6*, 860−867.
37. Lightning, L. K., Huang, H., Moenne-Loccoz, P., Loehr, T. M., Schuller, D. J., Poulos, T. L., and de Montellano, P. R. (2001) Disruption of an active site hydrogen bond converts human heme oxygenase-1 into a peroxidase, *J. Biol. Chem. 276*, 10612−10619.
38. Lad, L., Wang, J., Li, H., Friedman, J., Bhaskar, B., Ortiz de Montellano, P. R., and Poulos, T. L. (2003) Crystal structures of the ferric, ferrous, and ferrous-NO forms of the Asp140Ala mutant of human heme oxygenase-1: Catalytic implications, *J. Mol. Biol. 330*, 527−538.
39. Fujii, H., Zhang, X., Tomita, T., Ikeda-Saito, M., and Yoshida, T. (2001) A role for highly conserved carboxylate, aspartate-140, in oxygen activation and heme degradation by heme oxygenase-1, *J. Am. Chem. Soc. 123*, 6475−6484.
40. Matsui, T., Nakajima, A., Fujii, H., Matera, K. M., Migita, C. T., Yoshida, T., and Ikeda-Saito, M. (2005) O_2- and H_2O_2-dependent verdoheme degradation by heme oxygenase: Reaction mechanisms and potential physiological roles of the dual pathway degradation, *J. Biol. Chem. 280*, 36833−36840.

BI062264P